chapter

11

Subsonic Compressible Flow over Airfoils: Linear Theory

During the war a British engineer named Frank Whittle invented the jet engine, and deHavilland built the first production-type model. He produced a jet plane named Vampire, the first to exceed 500 mph. Then he built the experimental DH 108, and released it to young Geoffrey for test. In the first cautious trials the new plane behaved beautifully; but as Geoffrey stepped up the speed he unsuspectingly drew closer to an invisible wall in the sky then unknown to anyone, later named the sound barrier, which can destroy a plane not designed to pierce it. One evening he hit the speed of sound, and the plane disintegrated. Young Geoffrey's body was not found for ten days.

From the Royal Air Force Flying Review, as digested in Reader's Digest, 1959

11.1 Introduction

The above quotation refers to an accident which took place on September 27, 1946, when Geoffrey deHavilland, son of the famed British airplane designer Sir Geoffrey deHavilland, took the D. H. 108 Swallow up for an attack on the world's speed record. At that time, no airplane had flown at or beyond the speed of sound. The Swallow was an experimental jet-propelled aircraft with swept wings and no tail. During its first high-speed, low-level run, the Swallow encountered major compressibility problems and broke up in the air. deHavilland was killed instantly. This accident strengthened the opinion of many that Mach 1 stood as a barrier to manned flight and that no airplane would ever fly faster than the speed of sound. This myth of the "sound barrier" originated in the early 1930s. It was in full force by the time of the

Volta Conference in 1935 (see Section 7.1). In light of the opening quotation, the idea of a sound barrier was still being discussed in the popular literature as late as 1959, 12 years after the first successful supersonic flight by Captain Charles Yeager on October 14, 1947.

Of course, we know today that the sound barrier is indeed a myth; the supersonic transport Concorde flies at Mach 2, and some military aircraft are capable of Mach 3 and slightly beyond. The X-15 hypersonic research airplane has flown at Mach 7, and the Apollo lunar return capsule successfully reentered the earth's atmosphere at Mach 36. Supersonic flight is now an everyday occurrence. So, what caused the early concern about a sound barrier? In the present chapter, we develop a theory applicable to high-speed subsonic flight, and we see how the theory predicts a monotonically increasing drag going to infinity as $M_\infty \rightarrow 1$. It was this type of result that led some people in the early 1930s to believe that flight beyond the speed of sound was impossible. However, we also show in this chapter that the approximations made in the theory break down near Mach 1 and that in reality, although the drag coefficient at Mach 1 is large, it is still a manageable finite number.

Specifically, the purpose of this chapter is to examine the properties of two-dimensional airfoils at Mach numbers above 0.3, where we can no longer assume incompressible flow, but below Mach 1. That is, this chapter is an extension of the airfoil discussions in Chapter 4 (which applied to incompressible flow) to the high-speed subsonic regime.

In the process, we climb to a new tier in our study of compressible flow. If you survey our discussions so far of compressible flow, you will observe that they treat one-dimensional cases such as normal shock waves and flows in ducts. Even oblique shock waves, which are two- and three-dimensional in nature, depend only on the component of Mach number normal to the wave. Therefore, we have not been explicitly concerned with a multidimensional flow. As a consequence, note that the types of equations which allow an analysis of these flows are *algebraic equations*, and hence are relatively easy to solve in comparison with partial differential equations. In Chapters 8 to 10, we have dealt primarily with such algebraic equations. These algebraic equations were obtained by applying the integral forms of the conservation equations [Equations (2.48), (2.64), and (2.95)] to appropriate control volumes where the flow properties were uniform over the inflow and outflow faces of the control volume. However, for general two- and three-dimensional flows, we are usually not afforded such a luxury. Instead, we must deal directly with the governing equations in their partial differential equation form (see Chapter 2). Such is the nature of the present chapter. Indeed, for the remainder of our aerodynamic discussions in this book, we appeal mainly to the differential forms of the continuity, momentum, and energy equations [such as Equations (2.52), (2.113*a* to *c*), and (2.114)].

The road map for this chapter is given in Figure 11.1. We are going to return to the concept of a velocity potential, first introduced in Section 2.15. We are going to combine our governing equations so as to obtain a single equation simply in terms of the velocity potential; that is, we are going to obtain for compressible flow an equation analogous to Laplace's equation derived for incompressible flow in Section 3.7 [see Equation (3.40)]. However, unlike Laplace's equation, which is linear, the exact

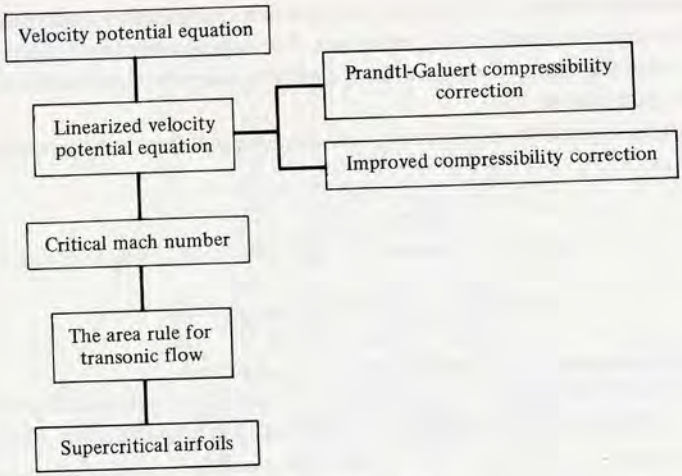

Figure 11.1 Road map for Chapter 11.

velocity potential equation for compressible flow is nonlinear. By making suitable approximations, we are able to linearize this equation and apply it to thin airfoils at small angles of attack. The results enable us to correct incompressible airfoil data for the effects of compressibility—so-called *compressibility corrections*. Finally, we conclude this chapter by discussing several practical aspects of airfoil and general wing-body aerodynamics at speeds near Mach 1.

11.2 The Velocity Potential Equation

The inviscid, compressible, subsonic flow over a body immersed in a uniform stream is *irrotational*; there is no mechanism in such a flow to start rotating the fluid elements (see Section 2.12). Thus, a velocity potential (see Section 2.15) can be defined. Since we are dealing with irrotational flow and the velocity potential, review Sections 2.12 and 2.15 before progressing further.

Consider two-dimensional, steady, irrotational, isentropic flow. A velocity potential, $\phi = \phi(x, y)$, can be defined such that [from Equation (2.154)]

$$\mathbf{V} = \nabla\phi \qquad \textbf{[11.1]}$$

or in terms of the cartesian velocity components,

$$u = \frac{\partial\phi}{\partial x} \qquad \textbf{[11.2a]}$$

$$v = \frac{\partial\phi}{\partial y} \qquad \textbf{[11.2b]}$$

Let us proceed to obtain an equation for ϕ which represents a combination of the continuity, momentum, and energy equations. Such an equation would be very useful, because it would be simply one governing equation in terms of one unknown, namely the velocity potential ϕ.

The continuity equation for steady, two-dimensional flow is obtained from Equation (2.52) as

$$\frac{\partial(\rho u)}{\partial x} + \frac{\partial(\rho v)}{\partial y} = 0 \qquad \textbf{[11.3]}$$

or

$$\rho\frac{\partial u}{\partial x} + u\frac{\partial \rho}{\partial x} + v\frac{\partial \rho}{\partial y} + \rho\frac{\partial v}{\partial y} = 0 \qquad \textbf{[11.4]}$$

Substituting Equations (11.2*a* and *b*) into (11.4), we have

$$\rho\frac{\partial^2\phi}{\partial x^2} + \frac{\partial\phi}{\partial x}\frac{\partial\rho}{\partial x} + \frac{\partial\phi}{\partial y}\frac{\partial\rho}{\partial y} + \rho\frac{\partial^2\phi}{\partial y^2} = 0$$

or

$$\rho\left(\frac{\partial^2\phi}{\partial x^2} + \frac{\partial^2\phi}{\partial y^2}\right) + \frac{\partial\phi}{\partial x}\frac{\partial\rho}{\partial x} + \frac{\partial\phi}{\partial y}\frac{\partial\rho}{\partial y} = 0 \qquad \textbf{[11.5]}$$

We are attempting to obtain an equation completely in terms of ϕ; hence, we need to eliminate ρ from Equation (11.5). To do this, consider the momentum equation in terms of Euler's equation:

$$dp = -\rho V\, dV \qquad \textbf{[3.12]}$$

This equation holds for a steady, compressible, inviscid flow and relates p and V along a streamline. It can readily be shown that Equation (3.12) holds in *any* direction throughout an irrotational flow, not just along a streamline (try it yourself). Therefore, from Equations (3.12) and (11.2*a* and *b*), we have

$$dp = -\rho V\, dV = -\frac{\rho}{2}d(V^2) = -\frac{\rho}{2}d(u^2 + v^2)$$

or

$$dp = -\frac{\rho}{2}d\left[\left(\frac{\partial\phi}{\partial x}\right)^2 + \left(\frac{\partial\phi}{\partial y}\right)^2\right] \qquad \textbf{[11.6]}$$

Recall that we are also considering the flow to be isentropic. Hence, any change in pressure dp in the flow is automatically accompanied by a corresponding isentropic change in density $d\rho$. Thus, by definition

$$\frac{dp}{d\rho} = \left(\frac{\partial p}{\partial \rho}\right)_s \qquad \textbf{[11.7]}$$

The right-hand side of Equation (11.7) is simply the square of the speed of sound. Thus, Equation (11.7) yields

$$dp = a^2\, d\rho \qquad \textbf{[11.8]}$$

Substituting Equation (11.8) for the left side of Equation (11.6), we have

$$d\rho = -\frac{\rho}{2a^2}d\left[\left(\frac{\partial\phi}{\partial x}\right)^2 + \left(\frac{\partial\phi}{\partial y}\right)^2\right] \qquad \textbf{[11.9]}$$

Considering changes in the x direction, Equation (11.9) directly yields

$$\frac{\partial \rho}{\partial x} = -\frac{\rho}{2a^2}\frac{\partial}{\partial x}\left[\left(\frac{\partial \phi}{\partial x}\right)^2 + \left(\frac{\partial \phi}{\partial y}\right)^2\right]$$

or

$$\frac{\partial \rho}{\partial x} = -\frac{\rho}{a^2}\left(\frac{\partial \phi}{\partial x}\frac{\partial^2 \phi}{\partial x^2} + \frac{\partial \phi}{\partial y}\frac{\partial^2 \phi}{\partial x \partial y}\right) \qquad \textbf{[11.10]}$$

Similarly, for changes in the y direction, Equation (11.9) gives

$$\frac{\partial \rho}{\partial y} = -\frac{\rho}{a^2}\left(\frac{\partial \phi}{\partial x}\frac{\partial^2 \phi}{\partial x \partial y} + \frac{\partial \phi}{\partial y}\frac{\partial^2 \phi}{\partial y^2}\right) \qquad \textbf{[11.11]}$$

Substituting Equations (11.10) and (11.11) into (11.5), canceling the ρ which appears in each term, and factoring out the second derivatives of ϕ, we obtain

$$\boxed{\left[1 - \frac{1}{a^2}\left(\frac{\partial \phi}{\partial x}\right)^2\right]\frac{\partial^2 \phi}{\partial x^2} + \left[1 - \frac{1}{a^2}\left(\frac{\partial \phi}{\partial y}\right)^2\right]\frac{\partial^2 \phi}{\partial y^2} - \frac{2}{a^2}\left(\frac{\partial \phi}{\partial x}\right)\left(\frac{\partial \phi}{\partial y}\right)\frac{\partial^2 \phi}{\partial x \partial y} = 0}$$

[11.12]

which is called the *velocity potential equation*. It is almost completely in terms of ϕ; only the speed of sound appears in addition to ϕ. However, a can be readily expressed in terms of ϕ as follows. From Equation (8.33), we have

$$a^2 = a_0^2 - \frac{\gamma - 1}{2}V^2 = a_0^2 - \frac{\gamma - 1}{2}(u^2 + v^2)$$

$$= a_0^2 - \frac{\gamma - 1}{2}\left[\left(\frac{\partial \phi}{\partial x}\right)^2 + \left(\frac{\partial \phi}{\partial y}\right)^2\right] \qquad \textbf{[11.13]}$$

Since a_0 is a known constant of the flow, Equation (11.13) gives the speed of sound a as a function of ϕ. Hence, substitution of Equation (11.13) into (11.12) yields a single partial differential equation in terms of the unknown ϕ. This equation represents a combination of the continuity, momentum, and energy equations. In principle, it can be solved to obtain ϕ for the flow field around any two-dimensional shape, subject of course to the usual boundary conditions at infinity and along the body surface. These boundary conditions on ϕ are detailed in Section 3.7, and are given by Equations (3.47*a* and *b*) and (3.48*b*).

Because Equation (11.12) [along with Equation (11.13)] is a single equation in terms of one dependent variable ϕ, the analysis of isentropic, irrotational, steady, compressible flow is greatly simplified—we only have to solve one equation instead of three or more. Once ϕ is known, all the other flow variables are directly obtained as follows:

1. Calculate u and v from Equations (11.2*a* and *b*).
2. Calculate a from Equation (11.13).
3. Calculate $M = V/a = \sqrt{u^2 + v^2}/a$.

4. Calculate T, p, and ρ from Equations (8.40), (8.42), and (8.43), respectively. In these equations, the total conditions T_0, p_0, and ρ_0 are known quantities; they are constant throughout the flow field and hence are obtained from the given freestream conditions.

Although Equation (11.12) has the advantage of being one equation with one unknown, it also has the distinct disadvantage of being a *nonlinear* partial differential equation. Such nonlinear equations are very difficult to solve analytically, and in modern aerodynamics, solutions of Equation (11.12) are usually sought by means of sophisticated finite-difference numerical techniques. Indeed, no general analytical solution of Equation (11.12) has been found to this day. Contrast this situation with that for incompressible flow, which is governed by Laplace's equation—a *linear* partial differential equation for which numerous analytical solutions are well known.

Given this situation, aerodynamicists over the years have made assumptions regarding the physical nature of the flow field which are designed to simplify Equation (11.12). These assumptions limit our considerations to the flow over slender bodies at small angles of attack. For subsonic and supersonic flows, these assumptions lead to an *approximate* form of Equation (11.12) which is linear, and hence can be solved analytically. These matters are the subject of the next section.

Keep in mind that, within the framework of steady, irrotational, isentropic flow, Equation (11.12) is *exact* and holds for all Mach numbers, from subsonic to hypersonic, and for all two-dimensional body shapes, thin and thick.

11.3 The Linearized Velocity Potential Equation

Consider the two-dimensional, irrotational, isentropic flow over the body shown in Figure 11.2. The body is immersed in a uniform flow with velocity V_∞ oriented in the x direction. At an arbitrary point P in the flow field, the velocity is $\mathbf{V}$ with the x and y components given by u and v, respectively. Let us now visualize the velocity $\mathbf{V}$ as the sum of the uniform flow velocity plus some extra increments in velocity. For example, the x component of velocity u in Figure 11.2 can be visualized as V_∞ plus an increment in velocity (positive or negative). Similarly, the y component of velocity v can be visualized as a simple increment itself, because the uniform flow has a zero component in the y direction. These increments are called *perturbations*, and

$$u = V_\infty + \hat{u} \qquad v = \hat{v}$$

where $\hat{u}$ and $\hat{v}$ are called the *perturbation velocities*. These perturbation velocities are not necessarily small; indeed, they can be quite large in the stagnation region in front of the blunt nose of the body shown in Figure 11.2. In the same vein, because $\mathbf{V} = \nabla\phi$, we can define a perturbation velocity potential $\hat{\phi}$ such that

$$\phi = V_\infty x + \hat{\phi}$$

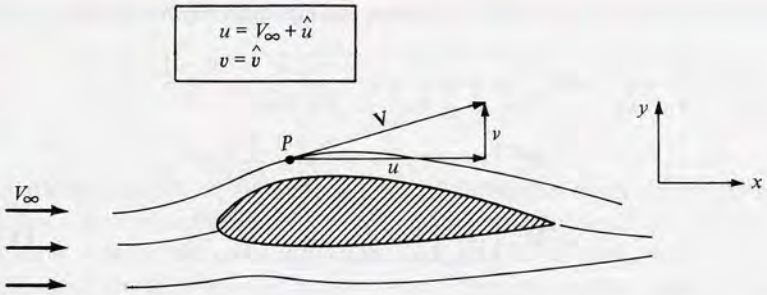

Figure 11.2 Uniform flow and perturbed flow.

where

$$\frac{\partial \hat{\phi}}{\partial x} = \hat{u}$$

$$\frac{\partial \hat{\phi}}{\partial y} = \hat{v}$$

Hence,

$$\frac{\partial \phi}{\partial x} = V_\infty + \frac{\partial \hat{\phi}}{\partial x} \qquad \frac{\partial \phi}{\partial y} = \frac{\partial \hat{\phi}}{\partial y}$$

$$\frac{\partial^2 \phi}{\partial x^2} = \frac{\partial^2 \hat{\phi}}{\partial x^2} \qquad \frac{\partial^2 \phi}{\partial y^2} = \frac{\partial^2 \hat{\phi}}{\partial y^2} \qquad \frac{\partial^2 \phi}{\partial x\, \partial y} = \frac{\partial^2 \hat{\phi}}{\partial x\, \partial y}$$

Substituting the above definitions into Equation (11.12), and multiplying by a^2, we obtain

$$\left[a^2 - \left(V_\infty + \frac{\partial \hat{\phi}}{\partial x}\right)^2\right] \frac{\partial^2 \hat{\phi}}{\partial x^2} + \left[a^2 - \left(\frac{\partial \hat{\phi}}{\partial y}\right)^2\right] \frac{\partial^2 \hat{\phi}}{\partial y^2} - 2\left(V_\infty + \frac{\partial \hat{\phi}}{\partial x}\right)\left(\frac{\partial \hat{\phi}}{\partial y}\right) \frac{\partial^2 \hat{\phi}}{\partial x\, \partial y} = 0 \qquad \textbf{[11.14]}$$

Equation (11.14) is called the *perturbation velocity potential equation*. It is precisely the same equation as Equation (11.12) except that it is expressed in terms of $\hat{\phi}$ instead of ϕ. It is still a nonlinear equation.

To obtain better physical insight in some of our subsequent discussion, let us recast Equation (11.14) in terms of the perturbation velocities. From the definition of $\hat{\phi}$ given earlier, Equation (11.14) can be written as

$$[a^2 - (V_\infty + \hat{u})^2] \frac{\partial \hat{u}}{\partial x} + (a^2 - \hat{v}^2) \frac{\partial \hat{v}}{\partial y} - 2(V_\infty + \hat{u})\hat{v} \frac{\partial \hat{u}}{\partial y} = 0 \qquad \textbf{[11.14a]}$$

From the energy equation in the form of Equation (8.32), we have

$$\frac{a_\infty^2}{\gamma - 1} + \frac{V_\infty^2}{2} = \frac{a^2}{\gamma - 1} + \frac{(V_\infty + \hat{u})^2 + \hat{v}^2}{2} \qquad \textbf{[11.15]}$$

Substituting Equation (11.15) into (11.14*a*), and algebraically rearranging, we obtain

$$(1-M_\infty^2)\frac{\partial \hat{u}}{\partial x}+\frac{\partial \hat{v}}{\partial y}=M_\infty^2\left[(\gamma+1)\frac{\hat{u}}{V_\infty}+\frac{\gamma+1}{2}\frac{\hat{u}^2}{V_\infty^2}+\frac{\gamma-1}{2}\frac{\hat{v}^2}{V_\infty^2}\right]\frac{\partial \hat{u}}{\partial x}$$
$$+M_\infty^2\left[(\gamma-1)\frac{\hat{u}}{V_\infty}+\frac{\gamma+1}{2}\frac{\hat{v}^2}{V_\infty^2}+\frac{\gamma-1}{2}\frac{\hat{u}^2}{V_\infty^2}\right]\frac{\partial \hat{v}}{\partial y}$$
$$+M_\infty^2\left[\frac{\hat{v}}{V_\infty}\left(1+\frac{\hat{u}}{V_\infty}\right)\left(\frac{\partial \hat{u}}{\partial y}+\frac{\partial \hat{v}}{\partial x}\right)\right] \qquad \textbf{[11.16]}$$

Equation (11.16) is still exact for irrotational, isentropic flow. Note that the left-hand side of Equation (11.16) is linear but the right-hand side is nonlinear. Also, keep in mind that the size of the perturbations $\hat{u}$ and $\hat{v}$ can be large or small; Equation (11.16) holds for both cases.

Let us now limit our considerations to *small* perturbations; that is, assume that the body in Figure 11.2 is a *slender* body at *small* angle of attack. In such a case, $\hat{u}$ and $\hat{v}$ will be small in comparison with V_∞. Therefore, we have

$$\frac{\hat{u}}{V_\infty},\ \frac{\hat{v}}{V_\infty} \ll 1 \qquad \frac{\hat{u}^2}{V_\infty^2},\ \frac{\hat{v}^2}{V_\infty^2} \lll 1$$

Keep in mind that products of $\hat{u}$ and $\hat{v}$ with their derivatives are also very small. With this in mind, examine Equation (11.16). Compare like terms (coefficients of like derivatives) on the left- and right-hand sides of Equation (11.16). We find

1. For $0 \le M_\infty \le 0.8$ or $M_\infty \ge 1.2$, the magnitude of

$$M_\infty^2\left[(\gamma+1)\frac{\hat{u}}{V_\infty}+\cdots\right]\frac{\partial \hat{u}}{\partial x}$$

is small in comparison with the magnitude of

$$(1-M_\infty^2)\frac{\partial \hat{u}}{\partial x}$$

Thus, *ignore* the former term.

2. For $M_\infty < 5$ (approximately),

$$M_\infty^2\left[(\gamma-1)\frac{\hat{u}}{V_\infty}+\cdots\right]\frac{\partial \hat{v}}{\partial y}$$

is small in comparison with $\partial \hat{v}/\partial y$. So ignore the former term. Also,

$$M_\infty^2\left[\frac{\hat{v}}{V_\infty}\left(1+\frac{\hat{u}}{V_\infty}\right)\left(\frac{\partial \hat{u}}{\partial y}+\frac{\partial \hat{v}}{\partial x}\right)\right] \approx 0$$

With the above order-of-magnitude comparisons, Equation (11.16) reduces to

$$(1-M_\infty^2)\frac{\partial \hat{u}}{\partial x}+\frac{\partial \hat{v}}{\partial y}=0 \qquad \textbf{[11.17]}$$

or in terms of the perturbation velocity potential,

$$\boxed{(1 - M_\infty^2)\frac{\partial^2 \hat{\phi}}{\partial x^2} + \frac{\partial^2 \hat{\phi}}{\partial y^2} = 0} \qquad \textbf{[11.18]}$$

Examine Equation (11.18). It is a *linear* partial differential equation, and therefore is inherently simpler to solve than its parent equation, Equation (11.16). However, we have paid a price for this simplicity. Equation (11.18) is no longer exact. It is only an approximation to the physics of the flow. Due to the assumptions made in obtaining Equation (11.18), it is reasonably valid (but not exact) for the following combined situations:

1. *Small* perturbation, that is, thin bodies at small angles of attack
2. *Subsonic* and *supersonic* Mach numbers

In contrast, Equation (11.18) is not valid for thick bodies and for large angles of attack. Moreover, it cannot be used for transonic flow, where $0.8 < M_\infty < 1.2$, or for hypersonic flow, where $M_\infty > 5$.

We are interested in solving Equation (11.18) in order to obtain the pressure distribution along the surface of a slender body. Since we are now dealing with approximate equations, it is consistent to obtain a linearized expression for the pressure coefficient—an expression which is approximate to the same degree as Equation (11.18), but which is extremely simple and convenient to use. The linearized pressure coefficient can be derived as follows.

First, recall the definition of the pressure coefficient C_p given in Section 1.5:

$$C_p \equiv \frac{p - p_\infty}{q_\infty} \qquad \textbf{[11.19]}$$

where $q_\infty = \frac{1}{2}\rho_\infty V_\infty^2 =$ dynamic pressure. The dynamic pressure can be expressed in terms of M_∞ as follows:

$$q_\infty = \frac{1}{2}\rho_\infty V_\infty^2 = \frac{1}{2}\frac{\gamma p_\infty}{\gamma p_\infty}\rho_\infty V_\infty^2 = \frac{\gamma}{2}p_\infty\left(\frac{\rho_\infty}{\gamma p_\infty}\right)V_\infty^2 \qquad \textbf{[11.20]}$$

From Equation (8.23), we have $a_\infty^2 = \gamma p_\infty/\rho_\infty$. Hence, Equation (11.20) becomes

$$q_\infty = \frac{\gamma}{2}p_\infty\frac{V_\infty^2}{a_\infty^2} = \frac{\gamma}{2}p_\infty M_\infty^2 \qquad \textbf{[11.21]}$$

Substituting Equation (11.21) into (11.19), we have

$$\boxed{C_p = \frac{2}{\gamma M_\infty^2}\left(\frac{p}{p_\infty} - 1\right)} \qquad \textbf{[11.22]}$$

Equation (11.22) is simply an alternate form of the pressure coefficient expressed in terms of M_∞. It is still an exact representation of the definition of C_p.

To obtain a linearized form of the pressure coefficient, recall that we are dealing with an adiabatic flow of a calorically perfect gas; hence, from Equation (8.39),

$$T + \frac{V^2}{2c_p} = T_\infty + \frac{V_\infty^2}{2c_p} \qquad \textbf{[11.23]}$$

Recalling from Equation (7.9) that $c_p = \gamma R/(\gamma - 1)$, Equation (11.23) can be written as

$$T - T_\infty = \frac{V_\infty^2 - V^2}{2\gamma R/(\gamma - 1)} \qquad \textbf{[11.24]}$$

Also, recalling that $a_\infty = \sqrt{\gamma R T_\infty}$, Equation (11.24) becomes

$$\frac{T}{T_\infty} - 1 = \frac{\gamma - 1}{2}\frac{V_\infty^2 - V^2}{\gamma R T_\infty} = \frac{\gamma - 1}{2}\frac{V_\infty^2 - V^2}{a_\infty^2} \qquad \textbf{[11.25]}$$

In terms of the perturbation velocities

$$V^2 = (V_\infty + \hat{u})^2 + \hat{v}^2$$

Equation (11.25) can be written as

$$\frac{T}{T_\infty} = 1 - \frac{\gamma - 1}{2a_\infty^2}(2\hat{u}V_\infty + \hat{u}^2 + \hat{v}^2) \qquad \textbf{[11.26]}$$

Since the flow is isentropic, $p/p_\infty = (T/T_\infty)^{\gamma/(\gamma-1)}$, and Equation (11.26) becomes

$$\frac{p}{p_\infty} = \left[1 - \frac{\gamma - 1}{2a_\infty^2}(2\hat{u}V_\infty + \hat{u}^2 + \hat{v}^2)\right]^{\gamma/(\gamma-1)}$$

or

$$\frac{p}{p_\infty} = \left[1 - \frac{\gamma - 1}{2}M_\infty^2\left(\frac{2\hat{u}}{V_\infty} + \frac{\hat{u}^2 + \hat{v}^2}{V_\infty^2}\right)\right]^{\gamma/(\gamma-1)} \qquad \textbf{[11.27]}$$

Equation (11.27) is still an exact expression. However, let us now make the assumption that the perturbations are small, that is, $\hat{u}/V_\infty \ll 1$, $\hat{u}^2/V_\infty^2 \lll 1$, and $\hat{v}^2/V_\infty^2 \lll 1$. In this case, Equation (11.27) is of the form

$$\frac{p}{p_\infty} = (1 - \varepsilon)^{\gamma/(\gamma-1)} \qquad \textbf{[11.28]}$$

where ε is small. From the binomial expansion, neglecting higher-order terms, Equation (11.28) becomes

$$\frac{p}{p_\infty} = 1 - \frac{\gamma}{\gamma - 1}\varepsilon + \cdots \qquad \textbf{[11.29]}$$

Comparing Equation (11.27) to (11.29), we can express Equation (11.27) as

$$\frac{p}{p_\infty} = 1 - \frac{\gamma}{2}M_\infty^2\left(\frac{2\hat{u}}{V_\infty} + \frac{\hat{u}^2 + \hat{v}^2}{V_\infty^2}\right) + \cdots \qquad \textbf{[11.30]}$$

Substituting Equation (11.30) into the expression for the pressure coefficient, Equation (11.22), we obtain

$$C_p = \frac{2}{\gamma M_\infty^2}\left[1 - \frac{\gamma}{2}M_\infty^2\left(\frac{2\hat{u}}{V_\infty} + \frac{\hat{u}^2 + \hat{v}^2}{V_\infty^2}\right) + \cdots - 1\right]$$

or

$$C_p = -\frac{2\hat{u}}{V_\infty} + \frac{\hat{u}^2 + \hat{v}^2}{V_\infty^2} \qquad \textbf{[11.31]}$$

Since $\hat{u}^2/V_\infty^2$ and $\hat{v}^2/V_\infty^2 \lll 1$, Equation (11.31) becomes

$$\boxed{C_p = -\frac{2\hat{u}}{V_\infty}} \qquad \textbf{[11.32]}$$

Equation (11.32) is the linearized form for the pressure coefficient; it is valid only for *small* perturbations. Equation (11.32) is consistent with the linearized perturbation velocity potential equation, Equation (11.18). Note the simplicity of Equation (11.32); it depends only on the x component of the velocity perturbation, namely, $\hat{u}$.

To round out our discussion on the basics of the linearized equations, we note that any solution to Equation (11.18) must satisfy the usual boundary conditions at infinity and at the body surface. At infinity, clearly $\hat{\phi}$ = constant; that is, $\hat{u} = \hat{v} = 0$. At the body, the flow-tangency condition holds. Let θ be the angle between the tangent to the surface and the freestream. Then, at the surface, the boundary condition is obtained from Equation (3.48*e*):

$$\tan\theta = \frac{v}{u} = \frac{\hat{v}}{V_\infty + \hat{u}} \qquad \textbf{[11.33]}$$

which is an exact expression for the flow-tangency condition at the body surface. A simpler, approximate expression for Equation (11.33), consistent with linearized theory, can be obtained by noting that for small perturbations, $\hat{u} \ll V_\infty$. Hence, Equation (11.33) becomes

$$\hat{v} = V_\infty \tan\theta$$

or

$$\boxed{\frac{\partial\hat{\phi}}{\partial y} = V_\infty \tan\theta} \qquad \textbf{[11.34]}$$

Equation (11.34) is an *approximate* expression for the flow-tangency condition at the body surface, with accuracy of the same order as Equations (11.18) and (11.32).

11.4 PRANDTL-GLAUERT COMPRESSIBILITY CORRECTION

The aerodynamic theory for incompressible flow over thin airfoils at small angles of attack was presented in Chapter 4. For aircraft of the period 1903–1940, such theory

was adequate for predicting airfoil properties. However, with the rapid evolution of high-power reciprocating engines spurred by World war II, the velocities of military fighter planes began to push close to 450 mi/h. Then, with the advent of the first operational jet-propelled airplanes in 1944 (the German Me 262), flight velocities took a sudden spurt into the 550 mi/h range and faster. As a result, the incompressible flow theory of Chapter 4 was no longer applicable to such aircraft; rather, high-speed airfoil theory had to deal with compressible flow. Because a vast bulk of data and experience had been collected over the years in low-speed aerodynamics, and because there was no desire to totally discard such data, the natural approach to high-speed subsonic aerodynamics was to search for methods that would allow relatively simple *corrections* to existing incompressible flow results which would approximately take into account the effects of compressibility. Such methods are called *compressibility corrections*. The first, and most widely known of these corrections is the Prandtl-Glauert compressibility correction, to be derived in this section. The Prandtl-Glauert method is based on the linearized perturbation velocity potential equation given by Equation (11.18). Therefore, it is limited to thin airfoils at small angles of attack. Moreover, it is purely a subsonic theory and begins to give inappropriate results at values of $M_\infty = 0.7$ and above.

Consider the subsonic, compressible, inviscid flow over the airfoil sketched in Figure 11.3. The shape of the airfoil is given by $y = f(x)$. Assume that the airfoil is thin and that the angle of attack is small; in such a case, the flow is reasonably approximated by Equation (11.18). Define

$$\beta^2 \equiv 1 - M_\infty^2$$

so that Equation (11.18) can be written as

$$\beta^2 \frac{\partial^2 \hat{\phi}}{\partial x^2} + \frac{\partial^2 \hat{\phi}}{\partial y^2} = 0 \qquad \textbf{[11.35]}$$

Let us transform the independent variables x and y into a new space, ξ and η, such that

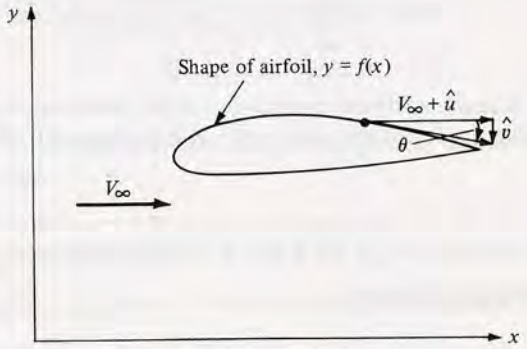

Figure 11.3 Airfoil in physical space.

$$\xi = x \qquad \textbf{[11.36a]}$$

$$\eta = \beta y \qquad \textbf{[11.36b]}$$

Moreover, in this transformed space, consider a new velocity potential $\bar{\phi}$ such that

$$\bar{\phi}(\xi, \eta) = \beta \hat{\phi}(x, y) \qquad \textbf{[11.36c]}$$

To recast Equation (11.35) in terms of the transformed variables, recall the chain rule of partial differentiation; that is,

$$\frac{\partial \hat{\phi}}{\partial x} = \frac{\partial \hat{\phi}}{\partial \xi}\frac{\partial \xi}{\partial x} + \frac{\partial \hat{\phi}}{\partial \eta}\frac{\partial \eta}{\partial x} \qquad \textbf{[11.37]}$$

and

$$\frac{\partial \hat{\phi}}{\partial y} = \frac{\partial \hat{\phi}}{\partial \xi}\frac{\partial \xi}{\partial y} + \frac{\partial \hat{\phi}}{\partial \eta}\frac{\partial \eta}{\partial y} \qquad \textbf{[11.38]}$$

From Equations (11.36*a* and *b*), we have

$$\frac{\partial \xi}{\partial x} = 1 \quad \frac{\partial \xi}{\partial y} = 0 \quad \frac{\partial \eta}{\partial x} = 0 \quad \frac{\partial \eta}{\partial y} = \beta$$

Hence, Equations (11.37) and (11.38) become

$$\frac{\partial \hat{\phi}}{\partial x} = \frac{\partial \hat{\phi}}{\partial \xi} \qquad \textbf{[11.39]}$$

$$\frac{\partial \hat{\phi}}{\partial y} = \beta \frac{\partial \hat{\phi}}{\partial \eta} \qquad \textbf{[11.40]}$$

Recalling Equation (11.36*c*), Equations (11.39) and (11.40) become

$$\frac{\partial \hat{\phi}}{\partial x} = \frac{1}{\beta}\frac{\partial \bar{\phi}}{\partial \xi} \qquad \textbf{[11.41]}$$

and

$$\frac{\partial \hat{\phi}}{\partial y} = \frac{\partial \bar{\phi}}{\partial \eta} \qquad \textbf{[11.42]}$$

Differentiating Equation (11.41) with respect to x (again using the chain rule), we obtain

$$\frac{\partial^2 \hat{\phi}}{\partial x^2} = \frac{1}{\beta}\frac{\partial^2 \bar{\phi}}{\partial \xi^2} \qquad \textbf{[11.43]}$$

Differentiating Equation (11.42) with respect to y, we find that the result is

$$\frac{\partial^2 \hat{\phi}}{\partial y^2} = \beta \frac{\partial^2 \bar{\phi}}{\partial \eta^2} \qquad \textbf{[11.44]}$$

Substitute Equations (11.43) and (11.44) into (11.35):

$$\beta^2 \frac{1}{\beta} \frac{\partial^2 \bar{\phi}}{\partial \xi^2} + \beta \frac{\partial^2 \bar{\phi}}{\partial \eta^2} = 0$$

or

$$\frac{\partial^2 \bar{\phi}}{\partial \xi^2} + \frac{\partial^2 \bar{\phi}}{\partial \eta^2} = 0 \qquad \textbf{[11.45]}$$

Examine Equation (11.45)—it should look familiar. Indeed, Equation (11.45) is Laplace's equation. Recall from Chapter 3 that Laplace's equation is the governing relation for *incompressible flow*. Hence, starting with a subsonic compressible flow in physical (x, y) space where the flow is represented by $\hat{\phi}(x, y)$ obtained from Equation (11.35), we have related this flow to an incompressible flow in transformed (ξ, η) space, where the flow is represented by $\bar{\phi}(\xi, \eta)$ obtained from Equation (11.45). The relation between $\bar{\phi}$ and $\hat{\phi}$ is given by Equation (11.36*c*).

Consider again the shape of the airfoil given in physical space by $y = f(x)$. The shape of the airfoil in the transformed space is expressed as $\eta = q(\xi)$. Let us compare the two shapes. First, apply the approximate boundary condition, Equation (11.34), in physical space, noting that $df/dx = \tan\theta$. We obtain

$$V_\infty \frac{df}{dx} = \frac{\partial \hat{\phi}}{\partial y} = \frac{1}{\beta} \frac{\partial \bar{\phi}}{\partial y} = \frac{\partial \bar{\phi}}{\partial \eta} \qquad \textbf{[11.46]}$$

Similarly, apply the flow-tangency condition in transformed space, which from Equation (11.34) is

$$V_\infty \frac{dq}{d\xi} = \frac{\partial \bar{\phi}}{\partial \eta} \qquad \textbf{[11.47]}$$

Examine Equations (11.46) and (11.47) closely. Note that the right-hand sides of these two equations are identical. Thus, from the left-hand sides, we obtain

$$\frac{df}{dx} = \frac{dq}{d\xi} \qquad \textbf{[11.48]}$$

Equation (11.48) implies that the shape of the airfoil in the transformed space is the same as in the physical space. Hence, the above transformation relates the compressible flow over an airfoil in (x, y) space to the incompressible flow in (ξ, η) space over the *same* airfoil.

The above theory leads to an immensely practical result, as follows. Recall Equation (11.32) for the linearized pressure coefficient. Inserting the above transformation into Equation (11.32), we obtain

$$C_p = \frac{2\hat{u}}{V_\infty} = -\frac{2}{V_\infty} \frac{\partial \hat{\phi}}{\partial x} = -\frac{2}{V_\infty} \frac{1}{\beta} \frac{\partial \bar{\phi}}{\partial x} = -\frac{2}{V_\infty} \frac{1}{\beta} \frac{\partial \bar{\phi}}{\partial \xi} \qquad \textbf{[11.49]}$$

Question: What is the significance of $\partial \bar{\phi}/\partial \xi$ in Equation (11.49)? Recall that $\bar{\phi}$ is the perturbation velocity potential for an incompressible flow in transformed space. Hence, from the definition of velocity potential, $\partial \bar{\phi}/\partial \xi = \bar{u}$, where $\bar{u}$ is a perturbation

velocity for the incompressible flow. Hence, Equation (11.49) can be written as

$$C_p = \frac{1}{\beta}\left(-\frac{2\bar{u}}{V_\infty}\right) \qquad \textbf{[11.50]}$$

From Equation (11.32), the expression $(-2\bar{u}/V_\infty)$ is simply the linearized pressure coefficient for the incompressible flow. Denote this incompressible pressure coefficient by $C_{p,0}$. Hence, Equation (11.50) gives

$$C_p = \frac{C_{p,0}}{\beta}$$

or recalling that $\beta \equiv \sqrt{1 - M_\infty^2}$, we have

$$\boxed{C_p = \frac{C_{p,0}}{\sqrt{1 - M_\infty^2}}} \qquad \textbf{[11.51]}$$

Equation (11.51) is called the *Prandtl-Glauert rule*; it states that, if we know the incompressible pressure distribution over an airfoil, then the compressible pressure distribution over the same airfoil can be obtained from Equation (11.51). Therefore, Equation (11.51) is truly a *compressibility correction* to incompressible data.

Consider the lift and moment coefficients for the airfoil. For an inviscid flow, the aerodynamic lift and moment on a body are simply integrals of the pressure distribution over the body, as described in Section 1.5. (If this is somewhat foggy in your mind, review Section 1.5 before progressing further.) In turn, the lift and moment *coefficients* are obtained from the integral of the pressure coefficient via Equations (1.15) to (1.19). Since Equation (11.51) relates the compressible and incompressible pressure coefficients, the same relation must therefore hold for lift and moment coefficients:

$$\boxed{c_l = \frac{c_{l,0}}{\sqrt{1 - M_\infty^2}}} \qquad \textbf{[11.52]}$$

$$\boxed{c_m = \frac{c_{m,0}}{\sqrt{1 - M_\infty^2}}} \qquad \textbf{[11.53]}$$

The Prandtl-Glauert rule, embodied in Equations (11.51) to (11.53), was historically the first compressibility correction to be obtained. As early as 1922, Prandtl was using this result in his lectures at Göttingen, although without written proof. The derivation of Equations (11.51) to (11.53) was first formally published by the British aerodynamicist, Hermann Glauert, in 1928. Hence, the rule is named after both men. The Prandtl-Glauert rule was used exclusively until 1939, when an improved compressibility correction was developed. Because of their simplicity, Equations (11.51) to (11.53) are still used today for initial estimates of compressibility effects.

Recall that the results of Chapters 3 and 4 proved that inviscid, incompressible flow over a closed, two-dimensional body theoretically produces zero drag—the well-known d'Alembert's paradox. Does the same paradox hold for inviscid, subsonic,

compressible flow? The answer can be obtained by again noting that the only source of drag is the integral of the pressure distribution. If this integral is zero for an incompressible flow, and since the compressible pressure coefficient differs from the incompressible pressure coefficient by only a constant scale factor, β, then the integral must also be zero for a compressible flow. Hence, d'Alembert's paradox also prevails for inviscid, subsonic, compressible flow. However, as soon as the freestream Mach number is high enough to produce locally supersonic flow on the body surface with attendant shock waves, as shown in Figure 1.37*b*, then a positive wave drag is produced, and d'Alembert's paradox no longer prevails.

Example 11.1

At a given point on the surface of an airfoil, the pressure coefficient is -0.3 at very low speeds. If the freestream Mach number is 0.6, calculate C_p at this point.

Solution

From Equation (11.51),

$$C_p = \frac{C_{p,0}}{\sqrt{1 - M^2}} = \frac{-0.3}{\sqrt{1 - (0.6)^2}} = \boxed{-0.375}$$

Example 11.2

From Chapter 4, the theoretical lift coefficient for a thin, symmetric airfoil in an incompressible flow is $c_l = 2\pi\alpha$. Calculate the lift coefficient for $M_\infty = 0.7$.

Solution

From Equation (11.52),

$$c_l = \frac{c_{l,0}}{\sqrt{1 - M_\infty^2}} = \frac{2\pi\alpha}{\sqrt{1 - (0.7)^2}} = \boxed{8.8\alpha}$$

Note: The effect of compressibility at Mach 0.7 is to increase the lift slope by the ratio $8.8/2\pi = 1.4$, or by 40 percent.

11.5 Improved Compressibility Corrections

The importance of accurate compressibility corrections reached new highs during the rapid increase in airplane speeds spurred by World War II. Efforts were made to improve upon the Prandtl-Glauert rule discussed in Section 11.4. Several of the more popular formulas are given below.

The Karman-Tsien rule states

$$C_p = \frac{C_{p,0}}{\sqrt{1 - M_\infty^2} + [M_\infty^2/(1 + \sqrt{1 - M_\infty^2})]C_{p,0}/2} \qquad \textbf{[11.54]}$$

This formula, derived in References 27 and 28, has been widely adopted by the aeronautical industry since World War II.

Laitone's rule states

$$C_p = \frac{C_{p,0}}{\sqrt{1 - M_\infty^2} + (M_\infty^2\{1 + [(\gamma - 1)/2]M_\infty^2\}/2\sqrt{1 - M_\infty^2})C_{p,0}} \quad \textbf{[11.55]}$$

This formula is more recent than either the Prandtl-Glauert or the Karman-Tsien rule; it is derived in Reference 29.

These compressibility corrections are compared in Figure 11.4, which also shows experimental data for the C_p variation with M_∞ at the 0.3-chord location on an NACA 4412 airfoil. Note that the Prandtl-Glauert rule, although the simplest to apply, underpredicts the experimental data, whereas the improved compressibility corrections are clearly more accurate. Recall that the Prandtl-Glauert rule is based on linear theory. In contrast, both the Laitone and Karman-Tsien rules attempt to account for some of the nonlinear aspects of the flow.

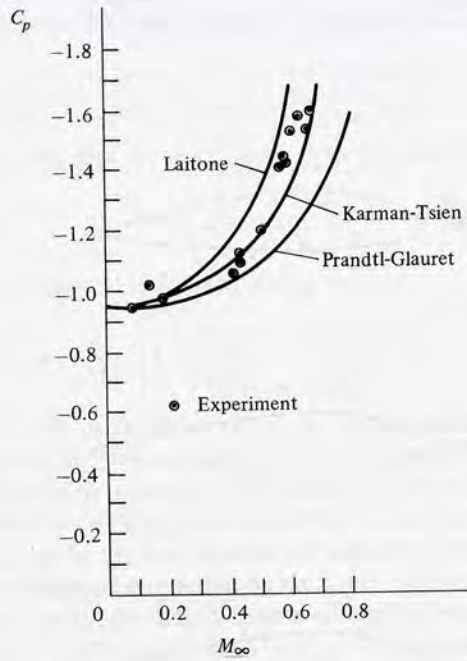

Figure 11.4 Several compressibility corrections compared with experimental results for an NACA 4412 airfoil at an angle of attack $\alpha = 1° 53'$. The experimental data are chosen for their historical significance; they are from NACA report no. 646, published in 1938 *(Reference 30)*. This was the first major NACA publication to address the compressibility problem in a systematic fashion; it covered work performed in the 2-ft high-speed tunnel at the Langley Aeronautical Laboratory and was carried out during 1935–1936.

11.6 Critical Mach Number

Return to the road map given in Figure 11.1. We have now finished our discussion of linearized flow and the associated compressibility corrections. Keep in mind that such linearized theory does *not* apply to the transonic flow regime, $0.8 \leq M_\infty \leq 1.2$. Transonic flow is highly nonlinear, and theoretical transonic aerodynamics is a challenging and sophisticated subject. For the remainder of this chapter, we deal with several aspects of transonic flow from a qualitative point of view. The theory of transonic aerodynamics is beyond the scope of this book.

Consider an airfoil in a low-speed flow, say, with $M_\infty = 0.3$, as sketched in Figure 11.5*a*. In the expansion over the top surface of the airfoil, the local flow Mach number M increases. Let point A represent the location on the airfoil surface

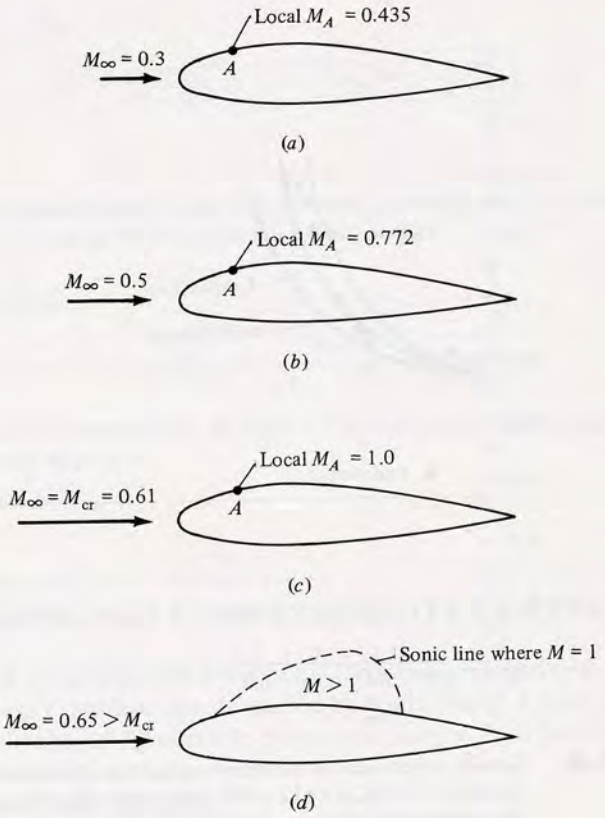

Figure 11.5 Definition of critical Mach number. Point A is the location of minimum pressure on the top surface of the airfoil. (See end-of-chapter Problem 11.7 for the calculation of the numbers in this figure.)

where the pressure is a minimum, hence where M is a maximum. In Figure 11.5*a*, let us say this maximum is $M_A = 0.435$. Now assume that we gradually increase the freestream Mach number. As M_∞ increases, M_A also increases. For example, if M_∞ is increased to $M = 0.5$, the maximum local value of M will be 0.772, as shown in Figure 11.5*b*. Let us continue to increase M_∞ until we achieve just the right value such that the local Mach number at the minimum pressure point equals 1, that is, such that $M_A = 1.0$, as shown in Figure 11.5*c*. When this happens, the freestream Mach number M_∞ is called the *critical Mach number*, denoted by M_{cr}. By definition, the critical Mach number is that *freestream* Mach number at which sonic flow is first achieved on the airfoil surface. In Figure 11.5*c*, $M_{cr} = 0.61$.

One of the most important problems in high-speed aerodynamics is the determination of the critical Mach number of a given airfoil, because at values of M_∞ slightly above M_{cr}, the airfoil experiences a dramatic increase in drag coefficient (discussed in Section 11.7). The purpose of the present section is to give a rather straightforward method for estimating M_{cr}.

Let p_∞ and p_A represent the static pressures in the freestream and at point A, respectively, in Figure 11.5. For isentropic flow, where the total pressure p_0 is constant, these static pressures are related through Equation (8.42) as follows:

$$\frac{p_A}{p_\infty} = \frac{p_A/p_0}{p_\infty/p_0} = \left(\frac{1 + [(\gamma - 1)/2]M_\infty^2}{1 + [(\gamma - 1)/2]M_A^2} \right)^{\gamma/(\gamma-1)} \qquad \textbf{[11.56]}$$

The pressure coefficient at point A is given by Equation (11.22) as

$$C_{p,A} = \frac{2}{\gamma M_\infty^2} \left(\frac{p_A}{p_\infty} - 1 \right) \qquad \textbf{[11.57]}$$

Combining Equations (11.56) and (11.57), we have

$$C_{p,A} = \frac{2}{\gamma M_\infty^2} \left[\left(\frac{1 + [(\gamma - 1)/2]M_\infty^2}{1 + [(\gamma - 1)/2]M_A^2} \right)^{\gamma/(\gamma-1)} - 1 \right] \qquad \textbf{[11.58]}$$

Equation (11.58) is useful in its own right; for a given freestream Mach number, it relates the local value of C_p to the local Mach number. [Note that Equation (11.58) is the compressible flow analogue of Bernoulli's equation, Equation (3.13), which for incompressible flow with a given freestream velocity and pressure relates the local pressure at a point in the flow to the local velocity at that point.] However, for our purposes here, we ask the question, What is the value of the local C_p when the local Mach number is unity? By definition, this value of the pressure coefficient is called the *critical pressure coefficient*, denoted by $C_{p,cr}$. For a given freestream Mach number M_∞, the value of $C_{p,cr}$ can be obtained by inserting $M_A = 1$ into Equation (11.58):

$$C_{p,cr} = \frac{2}{\gamma M_\infty^2} \left[\left(\frac{1 + [(\gamma - 1)/2]M_\infty^2}{1 + (\gamma - 1)/2} \right)^{\gamma/(\gamma-1)} - 1 \right] \qquad \textbf{[11.59]}$$

Equation (11.59) allows us to calculate the pressure coefficient at any point in the flow where the local Mach number is 1, for a given freestream Mach number M_∞. For example, if M_∞ is slightly greater than M_{cr}, say, $M_\infty = 0.65$ as shown in Figure

11.5*d*, then a finite region of supersonic flow will exist above the airfoil; Equation (11.59) allows us to calculate the pressure coefficient at only those points where $M = 1$, that is, at only those points that fall on the sonic line in Figure 11.5*d*. Now, returning to Figure 11.5*c*, when the freestream Mach number is precisely equal to the critical Mach number, there is only one point where $M = 1$, namely, point *A*. The pressure coefficient at point *A* will be $C_{p,\text{cr}}$, which is obtained from Equation (11.59). In this case, M_∞ in Equation (11.59) is precisely M_{cr}. Hence,

$$C_{p,\text{cr}} = \frac{2}{\gamma M_{\text{cr}}^2}\left[\left(\frac{1 + [(\gamma - 1)/2]M_{\text{cr}}^2}{1 + (\gamma - 1)/2}\right)^{\gamma/(\gamma-1)} - 1\right] \qquad \textbf{[11.60]}$$

Equation (11.60) shows that $C_{p,\text{cr}}$ is a unique function of M_{cr}; this variation is plotted as curve *C* in Figure 11.6. Note that Equation (11.60) is simply an aerodynamic relation for isentropic flow—it has no connection with the shape of a given airfoil. In this sense, Equation (11.60), and hence curve *C* in Figure 11.6, is a type of "universal relation" which can be used for all airfoils.

Equation (11.60), in conjunction with any one of the compressibility corrections given by Equations (11.51), (11.54), or (11.55), allows us to estimate the critical Mach number for a given airfoil as follows:

1. By some means, either experimental or theoretical, obtain the low-speed incompressible value of the pressure coefficient $C_{p,0}$ at the minimum pressure point on the given airfoil.
2. Using any of the compressibility corrections, Equation (11.51), (11.54), or (11.55), plot the variation of C_p with M_∞. This is represented by curve *B* in Figure 11.6.

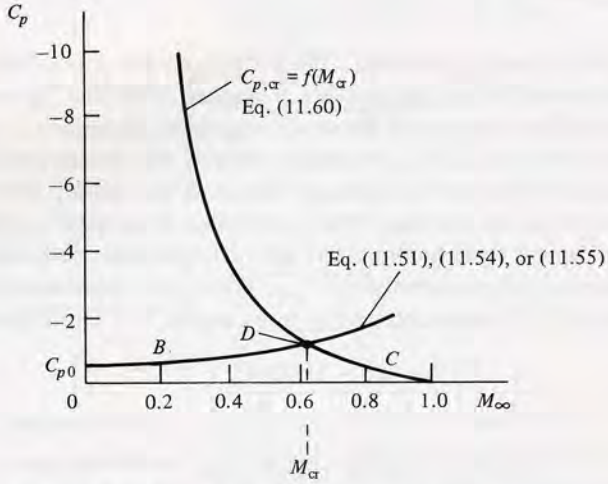

Figure 11.6 Estimation of critical Mach number.

3. Somewhere on curve B, there will be a single point where the pressure coefficient corresponds to locally sonic flow. Indeed, this point must coincide with Equation (11.60), represented by curve C in Figure 11.6. Hence, the *intersection* of curves B and C represents the point corresponding to sonic flow at the minimum pressure location on the airfoil. In turn, the value of M_∞ at this intersection is, by definition, the critical Mach number, as shown in Figure 11.6.

The graphical construction in Figure 11.6 is not an exact determination of M_{cr}. Although curve C is exact, curve B is approximate because it represents the approximate compressibility correction. Hence, Figure 11.6 gives only an estimation of M_{cr}. However, such an estimation is quite useful for preliminary design, and the results from Figure 11.6 are accurate enough for most applications.

Consider two airfoils, one thin and the other thick, as sketched in Figure 11.7. First consider the low-speed incompressible flow over these airfoils. The flow over the thin airfoil is only slightly perturbed from the freestream. Hence, the expansion over the top surface is mild, and $C_{p,0}$ at the minimum pressure point is a negative number of only small absolute magnitude, as shown in Figure 11.7. [Recall from Equation (11.32) that $C_p \propto \hat{u}$; hence, the smaller the perturbation, the smaller is the absolute magnitude of C_p.] In contrast, the flow over the thick airfoil experiences a large perturbation from the freestream. The expansion over the top surface is strong, and $C_{p,0}$ at the minimum pressure point is a negative number of large magnitude, as shown in Figure 11.7. If we now perform the same construction for each airfoil as given in Figure 11.6, we see that the thick airfoil will have a lower critical Mach number than

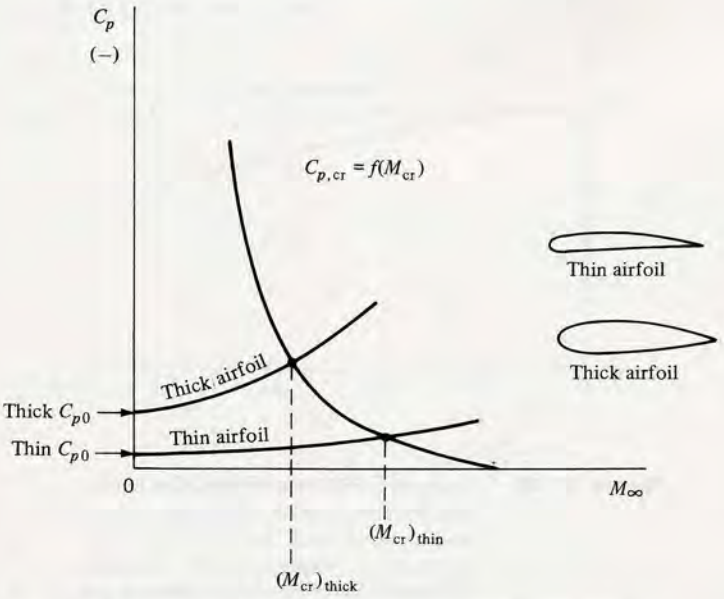

Figure 11.7 Effect of airfoil thickness on critical Mach number.

the thin airfoil. This is clearly illustrated in Figure 11.7. For high-speed airplanes, it is desirable to have M_{cr} as high as possible. Hence, modern high-speed subsonic airplanes are usually designed with relatively thin airfoils. (The development of the supercritical airfoil has somewhat loosened this criterion, as discussed in Section 11.8.) For example, the Gates Lear jet high-speed jet executive transport utilizes a 9 percent thick airfoil; contrast this with the low-speed Piper Aztec, a twin-engine propeller-driven general aviation aircraft designed with a 14 percent thick airfoil.

Example 11.3

In this example, we illustrate the estimation of the critical Mach number for an airfoil using (*a*) the graphical solution discussed in this section, and (*b*) an analytical solution using a closed-form equation obtained from a combination of Equations (11.51) and (11.60). Consider the NACA 0012 airfoil at zero angle of attack shown at the top of Figure 11.8. The pressure coefficient distribution over this airfoil, measured in a wind tunnel at low speed, is given at the

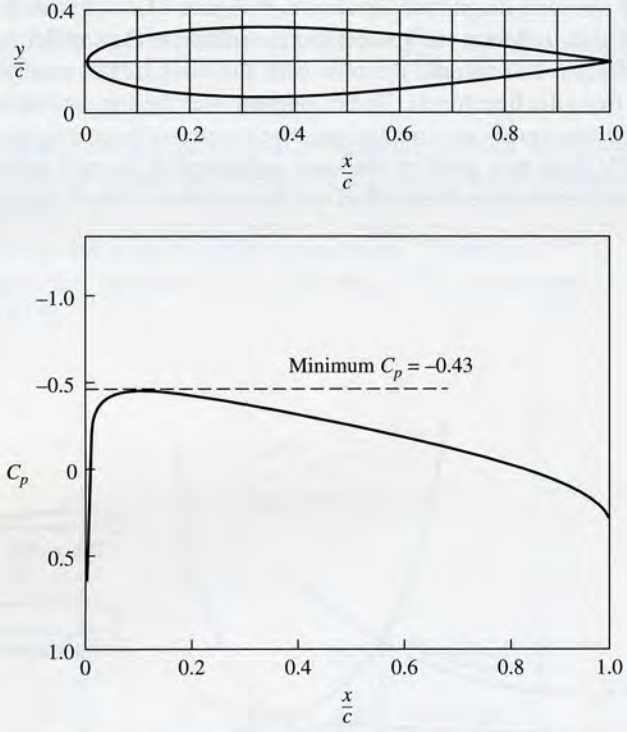

Figure 11.8 Low-speed pressure coefficient distribution over the surface of an NACA 0012 airfoil at zero angle of attack. Re = 3.65×10^6. (*Source:* R. J. Freuler and G. M. Gregorek, "An Evaluation of Four Single Element Airfoil Analytical Methods," in *Advanced Technology Airfoil Research*, NASA CP 2045, 1978, pp. 133–162.)

bottom of Figure 11.8. From this information, estimate the critical Mach number of the NACA 0012 airfoil at zero angle of attack.

Solution

(*a*) *Graphical Solution.* First, let us accurately plot the curve of $C_{p,\text{cr}}$ versus M_{cr} from Equation (11.60),

$$C_{p,\text{cr}} = \frac{2}{\gamma M_{\text{cr}}^2}\left[\left(\frac{1+[(\gamma-1)/2]M_{\text{cr}}^2}{1+(\gamma-1)/2}\right)^{\gamma/(\gamma-1)} - 1\right] \qquad \textbf{[11.60]}$$

For $\gamma = 1.4$, from Equation (11.60) we can tabulate

M_∞	0.4	0.5	0.6	0.7	0.8	0.9	1.0
$C_{p,\text{cr}}$	−3.66	−2.13	−1.29	−0.779	−0.435	−0.188	0

These numbers are plotted as curve C in Figure 11.9. Note that $C_{p,\text{cr}} = 0$ when $M_{\text{cr}} = 1.0$. This makes physical sense; if the free stream Mach number is already 1, then no change in the pressure is required to achieve Mach 1 at a local point in the flow, and hence the pressure difference $(p_{\text{cr}} - p_\infty)$ is zero and $C_{p,\text{cr}} = 0$.

Following the three-step procedure mentioned earlier, in step one we obtain the low-speed incompressible value of the minimum pressure coefficient $(C_{p,0})_{\text{min}}$ from the pressure coefficient distribution given in Figure 11.8. The *minimum* value of C_p on the surface is −0.43. Following step two, in Equation (11.51), $(C_{p,0})_{\text{min}} = -0.43$, and we have from Equation (11.51),

$$(C_p)_{\text{min}} = \frac{(C_{p,0})_{\text{min}}}{\sqrt{1-M_\infty^2}} = \frac{-0.43}{\sqrt{1-M_\infty^2}} \qquad \textbf{[11.61]}$$

Some values of $(C_p)_{\text{min}}$ are tabulated below

M_∞	0	0.2	0.4	0.6	0.8
$(C_p)_{\text{min}}$	−0.43	−0.439	−0.469	−0.538	−0.717

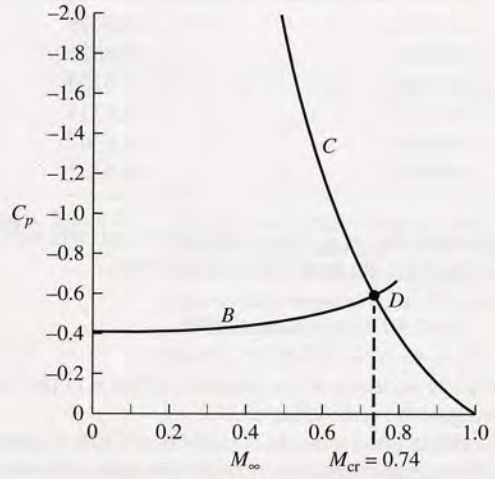

Figure 11.9 Graphical solution for the critical Mach number.

Following step three, these values are plotted as Curve B in Figure 11.9. The intersection of curves B and C is at point D. The freestream Mach number associated with point D is the critical Mach number for the NACA 0012 airfoil. From Figure 11.9, we have

$$\boxed{M_{cr} = 0.74}$$

(*b*) *Analytical Solution.* In Figure 11.9, curve B is given by Equation (11.61)

$$(C_p)_{min} = \frac{-0.43}{\sqrt{1 - M_\infty^2}} \qquad \textbf{[11.61]}$$

At the intersection point D, $(C_p)_{min}$ in Equation (11.61) is the critical pressure coefficient and M_∞ is the critical Mach number

$$C_{p,cr} = \frac{-0.43}{\sqrt{1 - M_{cr}^2}} \quad \text{(at point } D\text{)} \qquad \textbf{[11.62]}$$

Also, at point D the value of $C_{p,cr}$ is given by Equation (11.60). Hence, *at point D* we can equate the right-hand sides of Equations (11.62) and (11.60),

$$\frac{-0.43}{\sqrt{1 - M_{cr}^2}} = \frac{2}{\gamma M_{cr}^2}\left[\left(\frac{1 + [(\gamma - 1)/2]M_{cr}^2}{1 + (\gamma - 1)/2}\right)^{\gamma/\gamma - 1} - 1\right] \qquad \textbf{[11.63]}$$

Equation (11.63) is one equation with one unknown, namely, M_{cr}. The solution of Equation (11.63) gives the value of M_{cr} associated with the intersection point D in Figure 11.9, that is, the solution of Equation (11.63) is the critical Mach number for the NACA 0012 airfoil. Since M_{cr} appears in a complicated fashion on both sides of Equation (11.63), we solve the equation by trial-and-error by assuming different values of M_{cr}, calculating the values of both sides of Equation (11.63), and iterating until we find a value of M_{cr} that results in both the right and left sides being the same value.

M_{cr}	$\dfrac{-0.43}{\sqrt{1 - M_{cr}^2}}$	$\dfrac{2}{\gamma M_{cr}^2}\left[\left(\dfrac{1 + [(\gamma - 1)/2]M_{cr}^2}{1 + (\gamma - 1)/2}\right)^{\gamma/\gamma - 1} - 1\right]$
0.72	−0.6196	−0.6996
0.73	−0.6292	−0.6621
0.74	−0.6393	−0.6260
0.738	−0.6372	−0.6331
0.737	−0.6362	−0.6367
0.7371	−0.6363	−0.6363

To four-place accuracy, when $M_{cr} = 0.7371$, both the left and right sides of Equation (11.63) have the same value. Therefore, the analytical solution yields

$$\boxed{M_{cr} = 0.7371}$$

Note: Within the two-place accuracy of the graphical solution in part (a), both the graphical and analytical solutions give the same value of M_{cr}.

Question: How accurate is the estimate of the critical Mach number in this example? To answer this question, we examine some experimental pressure coefficient distributions for the NACA 0012 airfoil obtained at higher freestream Mach numbers. Wind tunnel measurements of the surface pressure distributions for this airfoil at zero angle of attack in a high-speed flow are shown in Figure 11.10; for Figure 11.10*a*, $M_\infty = 0.575$, and for Figure 11.10*b*,

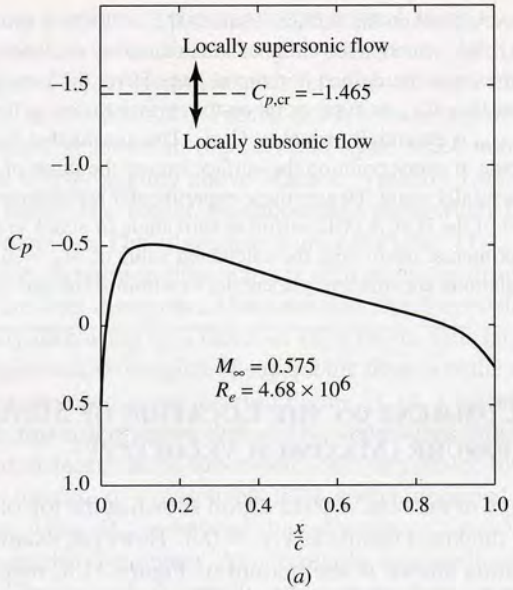

Figure 11.10 Wind tunnel measurements of surface pressure coefficient distribution for the NACA 0012 airfoil at zero angle of attack. Experimental data of Frueler and Gregorek, NASA CP 2045. (*a*) $M_\infty = 0.575$, (*b*) $M_\infty = 0.725$.

$M_\infty = 0.725$. In Figure 11.10*a*, the value of $C_{p,cr} = -1.465$ at $M_\infty = 0.575$ is shown as the dashed horizontal line. From the definition of critical pressure coefficient, any local value of C_p above this horizontal line corresponds to locally supersonic flow, and any local value below the horizontal line corresponds to locally subsonic flow. Clearly from the measured surface pressure coefficient distribution at $M_\infty = 0.575$ shown in Figure 11.10*a*, the flow is

locally subsonic at every point on the surface. Hence, $M_\infty = 0.575$ is *below* the critical Mach number. In Figure 11.10*b*, which is for a higher Mach number, the value of $C_{p,cr} = -0.681$ at $M_\infty = 0.725$ is shown as the dashed horizontal line. Here, the local pressure coefficient on the airfoil is higher than $C_{p,cr}$ at every point on the surface *except* at the point of minimum pressure, where $(C_p)_{min}$ is essentially equal to $C_{p,cr}$. This means that for $M_\infty = 0.725$, the flow is locally subsonic at every point on the surface *except* the point of minimum pressure, where the flow is essentially sonic. Hence, these experimental measurements indicate that the critical Mach number of the NACA 0012 airfoil at zero angle of attack is approximately 0.73. Comparing this experimental result with the calculated value of $M_{cr} = 0.74$ in this example, we see that our calculations are amazingly accurate, to within about one percent.

11.6.1 A Comment on the Location of Minimum Pressure (Maximum Velocity)

Examining the shape of the NACA 0012 airfoil shown at the top of Figure 11.8, note that the maximum thickness occurs at $x/c = 0.3$. However, examining the pressure coefficient distribution shown at the bottom of Figure 11.8, note that the point of minimum pressure occurs on the surface at $x/c = 0.11$, considerably ahead of the point of maximum thickness. This is a graphic illustration of the general fact that the point of minimum pressure (hence maximum velocity) does *not* correspond to the location of maximum thickness of the airfoil. Intuition might at first suggest that, at least for a symmetric airfoil at zero degrees angle of attack, the location of minimum pressure (maximum velocity) on the surface might be at the maximum thickness of the airfoil, but our intuition would be completely wrong. Nature places the maximum velocity at a point which satisfies the physics of the *whole flow field*, not just what is happening in a local region of the flow. The point of maximum velocity is dictated by the *complete* shape of the airfoil, not just by the shape in a local region.

We also note that it is implicit in the approximate compressibility corrections discussed in Sections 11.4 and 11.5, and their use for the estimation of the critical Mach number as discussed in Section 11.6, that the point of minimum pressure remains at a fixed location on the body surface as M_∞ is increased from a very low to a high subsonic value. This is indeed approximately the case. Examine the experimental pressure distributions in Figures 11.8 and 11.10, which are for three different Mach numbers ranging from a low, incompressible value (Figure 11.8) to $M_\infty = 0.725$ (Figure 11.10*b*). Note that in each case the minimum pressure point is at the same approximate location, that is, at $x/c = 0.11$.

11.7 Drag-Divergence Mach Number: The Sound Barrier

Imagine that we have a given airfoil at a fixed angle of attack in a wind tunnel, and we wish to measure its drag coefficient c_d as a function of M_∞. To begin with, we measure the drag coefficient at low subsonic speed to be $c_{d,0}$, shown in Figure 11.11. Now, as we gradually increase the freestream Mach number, we observe that

c_d remains relatively constant all the way to the critical Mach number, as illustrated in Figure 11.11. The flow fields associated with points a, b, and c in Figure 11.11 are represented by Figure 11.5a, b, and c, respectively. As we very carefully increase M_∞ slightly above M_{cr}, say, to point d in Figure 11.11, a finite region of supersonic flow appears on the airfoil, as shown in Figure 11.5d. The Mach number in this bubble of supersonic flow is only slightly above Mach 1, typically 1.02 to 1.05. However, as we continue to nudge M_∞ higher, we encounter a point where the drag coefficient suddenly starts to increase. This is given as point e in Figure 11.11. The value of M_∞ at which this sudden increase in drag starts is defined as the *drag-divergence Mach number*. Beyond the drag-divergence Mach number, the drag coefficient can become very large, typically increasing by a factor of 10 or more. This large increase in drag is associated with an extensive region of supersonic flow over the airfoil, terminating in a shock wave, as sketched in the insert in Figure 11.11. Corresponding to point f on the drag curve, this insert shows that as M_∞ approaches unity, the flow on both the top and bottom surfaces can be supersonic, both terminated by shock waves. For example, consider the case of a reasonably thick airfoil, designed originally for low-speed applications, when M_∞ is beyond drag-divergence; in such a case, the local Mach number can reach 1.2 or higher. As a result, the terminating shock waves can be relatively strong. These shocks generally cause severe flow separation downstream of the shocks, with an attendant large increase in drag.

Now, put yourself in the place of an aeronautical engineer in 1936. You are familiar with the Prandtl-Glauert rule, given by Equation (11.51). You recognize that as $M_\infty \to 1$, this equation shows the absolute magnitude of C_p approaching

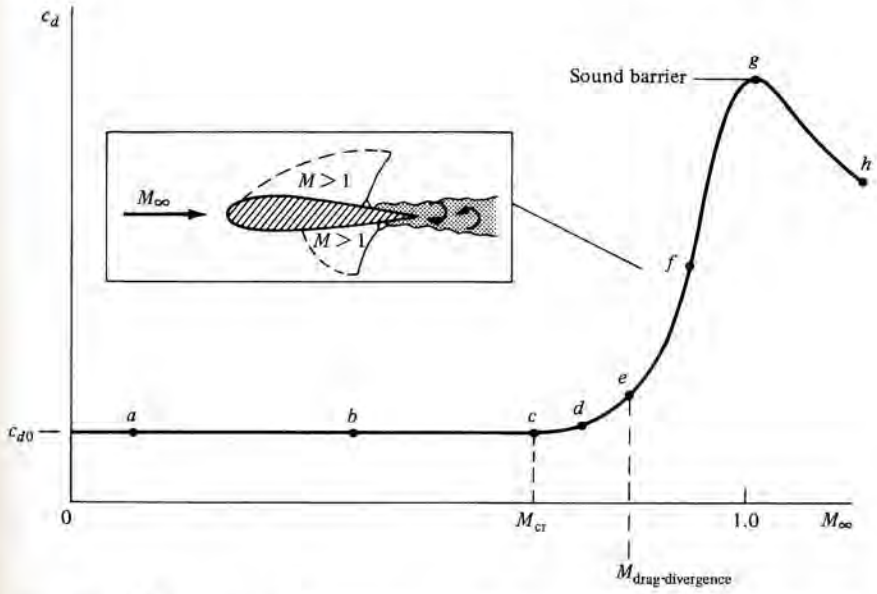

Figure 11.11 Sketch of the variation of profile drag coefficient with freestream Mach number, illustrating the critical and drag-divergence Mach numbers and showing the large drag rise near Mach 1.

infinity. This hints at some real problems near Mach 1. Furthermore, you know of some initial high-speed subsonic wind-tunnel tests that have generated drag curves which resemble the portion of Figure 11.11 from points a to f. How far will the drag coefficient increase as we get closer to $M_\infty = 1$? Will c_d go to infinity? At this stage, you might be pessimistic. You might visualize the drag increase to be so large that no airplane with the power plants existing in 1936, or even envisaged for the future, could ever overcome this "barrier." It was this type of thought that led to the popular concept of a sound barrier and that prompted many people to claim that humans would never fly faster than the speed of sound.

Of course, today we know the sound barrier was a myth. We cannot use the Prandtl-Glauert rule to argue that c_d will become infinite at $M_\infty = 1$, because the Prandtl-Glauert rule is invalid at $M_\infty = 1$ (see Sections 11.3 and 11.4). Moreover, early transonic wind-tunnel tests carried out in the late 1940s clearly indicated that c_d peaks at or around Mach 1 and then actually decreases as we enter the supersonic regime, as shown by points g and h in Figure 11.11. All we need is an aircraft with an engine powerful enough to overcome the large drag rise at Mach 1. The myth of the sound barrier was finally put to rest on October 14, 1947, when Captain Charles (Chuck) Yeager became the first human being to fly faster than sound in the sleek, bullet-shaped Bell XS-1. This rocket-propelled research aircraft is shown in Figure 11.12. Of course, today supersonic flight is a common reality; we have

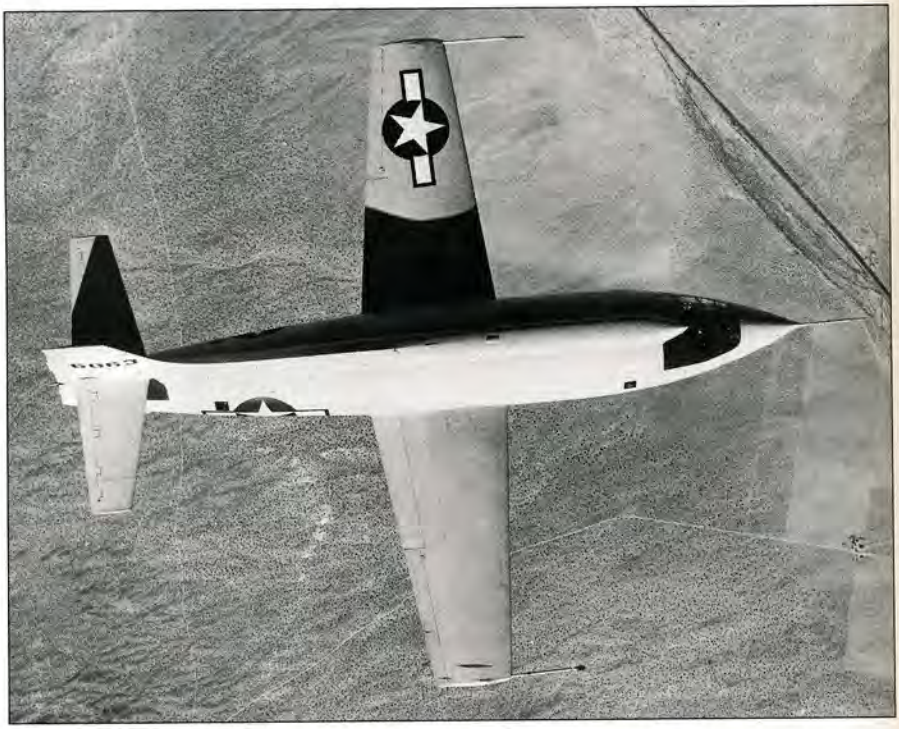

Figure 11.12 The Bell XS-1—the first manned airplane to fly faster than sound, October 14, 1947. *(Courtesy of the National Air and Space Museum.)*

jet engines powerful enough to accelerate military fighters through Mach 1 flying straight up! Such airplanes can fly at Mach 3 and beyond. Indeed, we are limited only by aerodynamic heating at high speeds (and the consequent structural problems). Right now, NASA is conducting research on supersonic combustion ramjet engines for flight at Mach 5 and higher (see the Design Box at the end of Section 9.6). Keep in mind, however, that because of the large power requirements for very high-speed flight, the fuel consumption becomes large. In today's energy-conscious world, this constraint can be as much a barrier to high-speed flight as the sound barrier was once envisaged.

Since 1945, research in transonic aerodynamics has focused on reducing the large drag rise shown in Figure 11.11. Instead of living with a factor of 10 increase in drag at Mach 1, can we reduce it to a factor of 2 or 3? This is the subject of the remaining sections of this chapter.

DESIGN BOX

In order to cope with the large drag rise near Mach one, as seen in Figure 11.11, the designers of high-speed airplanes after World War II utilized two aerodynamic design features to increase the critical Mach number, and hence the drag-divergence Mach number, for such aircraft. These two features are now classic and are discussed here.

The first design ploy was the use of *thin airfoil sections* on the airplane wing. We have already discussed that, everything else being equal, the thinner is the airfoil the higher is the critical Mach number; this is shown in Figure 11.7. This phenomena was observed as early as 1918 by two research engineers, F. W. Caldwell and E. N. Fales, at the Army's McCook Field in Dayton, Ohio, and was solidly confirmed by various experiments during the 1920s and 1930s. More historical details are given in Section 11.11, and the detailed story of the early research in the twentieth century on compressibility effects is told in Reference 62. Indeed, the Bell X-1 (Figure 11.12) was designed with the full knowledge of the importance of thin airfoils. As a result, the X-1 was designed with two sets of wings, one with a 10 percent thick airfoil for more routine flights and another with an 8 percent thick airfoil for flights intended to penetrate through Mach 1. The airfoil sections for the two wings were NACA 65-110 and NACA 65-108, respectively. These wings were much thinner than conventional airplanes at that time, which had wing thickness typically of 15 percent or higher. Moreover, the horizontal tail was even thinner, utilizing a 6-percent thick NACA 65-006 airfoil section. This was done to ensure that when the wing encountered major compressibility effects, the horizontal tail and elevator would still be free of such problems and would be functional for stability and control. However, hedging their bets, the Bell engineers also made the tail all-moving, that is, the incidence angle of the complete horizontal tail surface could be changed in flight in case elevator effectiveness was lost, and to help trim the airplane as it flew through Mach one. Chuck Yeager made good use of this all-moving tail feature during his history-making flights in the X-1.

The use of thin airfoils on high-speed aircraft is almost a standard design practice today. The design trend to thin airfoils is illustrated in Figure 11.13, which shows the variation of airfoil thickness for different airplanes as a function of their design Mach number. Clearly, as M_∞ increases, the trend is towards thinner wings.

The second design ploy was the use of swept wings. The story surrounding the history of the swept wing concept is told in Reference 62; the invention of the concept is shared by two people, the German engineer Adolf Busemann in 1935 and the American aerodynamicist R. T. Jones who independently conceived the idea in 1945. There are several ways of explaining how a swept wing works (e.g., see Reference 2). However, for our purposes here we will explain the benefit of a swept wing using the ideas set forth about thin airfoils, as discussed above.

(continued)

Finally, we note some compressibility corrections that apply to Equations (5.69), (5.81), and (5.82) given earlier for the estimation of the lift slope for high aspect ratio straight wings, low aspect ratio straight wings, and swept wings respectively. These equations apply to low-speed, incompressible flow. The Prandtl-Glauert rule for an airfoil section expressed in terms of pressure coefficient as given by Equation (11.51) also holds for the lift slope for the airfoil. Letting a_0 be the lift slope for an infinite wing for incompressible flow, and $a_{0,\text{comp}}$ be the lift slope for an infinite wing in a subsonic compressible flow, from the Prandtl-Glauert rule we have

$$a_{0,\text{comp}} = \frac{a_0}{\sqrt{1 - M_\infty^2}} \qquad \textbf{[11.64]}$$

We assume that Equation (5.70) relating the lift slope of a finite wing to that for an infinite wing, as obtained from Prandtl's lifting line theory, holds for subsonic compressible flow as well. Letting the term $(1 + \tau)^{-1}$ in Equation (5.70) be replaced by a span efficiency factor for lift slope denoted by e_1, where $e_1 = (1 + \tau)^{-1}$, and denoting the compressible lift slope for the finite wing by a_{comp}, the compressible analogue of Equation (5.70) is

$$a_{\text{comp}} = \frac{a_{0,\text{comp}}}{1 + a_{0,\text{comp}}/(\pi e_1 \text{AR})} \qquad \textbf{[11.65]}$$

Substituting Equation (11.64) into Equation (11.65), and simplifying, we obtain

$$\boxed{a_{\text{comp}} = \frac{a_0}{\sqrt{1 - M_\infty^2} + a_0/(\pi e_1 \text{AR})}} \qquad \textbf{[11.66]}$$

Equation (11.66) is an equation for estimating the lift slope for a *high-aspect-ratio straight wing* in a compressible flow with a subsonic M_∞ from the known lift slope for an infinite wing in an incompressible flow a_0.

Helmbold's equation for low-aspect-ratio straight wings for incompressible flow, Equation (5.81), can be modified for compressibility effects by replacing a_0 in that equation by $a_0/\sqrt{1 - M_\infty^2}$, yielding

$$\boxed{a_{\text{comp}} = \frac{a_0}{\sqrt{1 - M_\infty^2 + [a_0/(\pi e_1 \text{AR})]^2} + a_0/(\pi \text{AR})}} \qquad \textbf{[11.67]}$$

Equation (11.67) is an equation for estimating the lift slope for a *low-aspect-ratio straight wing* in a compressible flow with a subsonic M_∞ from the known lift slope for an infinite wing in an incompressible flow a_0.

Finally, Equation (5.82) for a swept wing can be modified for compressibility effects by replacing a_0 in that equation by $a_0/\sqrt{1 - (M_{\infty,n})^2}$ where $M_{\infty,n}$ is the component of the freestream Mach number perpendicular to the half-chord line of the swept wing. If the half-chord line is swept by the angle Λ, then $M_{\infty,n} = M_\infty \cos \Lambda$. Hence, replace a_0 in Equation (5.82) with $a_0/\sqrt{1 - M_\infty^2 \cos^2 \Lambda}$. The result is

$$\boxed{a_{\text{comp}} = \frac{a_0 \cos \Lambda}{\sqrt{1 - M_\infty^2 \cos^2 \Lambda + [(a_0 \cos \Lambda)/(\pi \text{AR})]^2} + (a_0 \cos \Lambda)/(\pi \text{AR})}} \qquad \textbf{[11.68]}$$

Equation (11.68) is an equation for estimating the lift slope for a *swept wing* in a compressible flow with a subsonic M_∞ from the known lift slope for an infinite wing in an incompressible flow a_0.

11.8 THE AREA RULE

In addition to the classic approaches of using thin airfoils and swept wings to cope with the large drag rise near Mach 1, in recent years two rather revolutionary concepts have helped greatly to break down the "sound barrier" near and beyond the speed of

sound. One of these—the area rule—is discussed in this section; the other—the supercritical airfoil—is the subject of Section 11.9.

For a moment, let us expand our discussion from two-dimensional airfoils to a consideration of a complete airplane. In this section, we introduce a design concept which has effectively reduced the drag rise near Mach 1 for a complete airplane.

As stated before, the first practical jet-powered aircraft appeared at the end of World War II in the form of the German Me 262. This was a subsonic fighter plane with a top speed near 550 mi/h. The next decade saw the design and production of many types of jet aircraft—all limited to subsonic flight by the large drag near Mach 1. Even the "century" series of fighter aircraft designed to give the U.S. Air Force supersonic capability in the early 1950s, such as the Convair F-102 delta-wing airplane, ran into difficulty and could not at first readily penetrate the sound barrier in level flight. The thrust of jet engines at that time simply could not overcome the large peak drag near Mach 1.

A planview, cross section, and area distribution (cross-sectional area versus distance along the axis of the airplane) for a typical airplane of that decade are sketched in Figure 11.16. Let A denote the total cross-sectional area at any given station. Note that the cross-sectional area distribution experiences some abrupt changes along the axis, with discontinuities in both A and dA/dx in the regions of the wing.

In contrast, for almost a century, it was well known by ballisticians that the speed of a supersonic bullet or artillery shell with a *smooth* variation of cross-sectional area

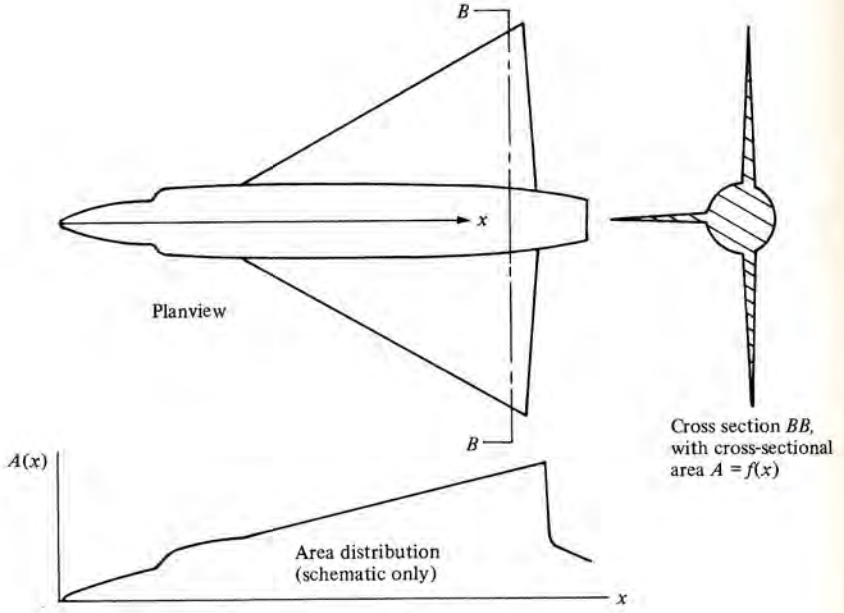

Figure 11.16 A schematic of a non-area-ruled aircraft.

was higher than projectiles with abrupt or discontinuous area distributions. In the mid-1950s, an aeronautical engineer at the NACA Langley Aeronautical Laboratory, Richard T. Whitcomb, put this knowledge to work on the problem of transonic flight of airplanes. Whitcomb reasoned that the variation of cross-sectional area for an airplane should be smooth, with no discontinuities. This meant that, in the region of the wings and tail, the fuselage cross-sectional area should decrease to compensate for the addition of the wing and tail cross-sectional area. This led to a "coke bottle" fuselage shape, as shown in Figure 11.17. Here, the planview and area distribution are shown for an aircraft with a relatively smooth variation of $A(x)$. This design philosophy is called the *area rule*, and it successfully reduced the peak drag near Mach 1 such that practical airplanes could fly supersonically by the mid-1950s. The variations of drag coefficient with M_∞ for an area-ruled and non-area-ruled airplane are schematically compared in Figure 11.18; typically, the area rule leads to a factor-of-2 reduction in the peak drag near Mach 1.

The development of the area rule was a dramatic breakthrough in high-speed flight, and it earned a substantial reputation for Richard Whitcomb—a reputation which was to be later garnished by a similar breakthrough in transonic airfoil design, to be discussed in Section 11.9. The original work on the area rule was presented by Whitcomb in Reference 31, which should be consulted for more details.

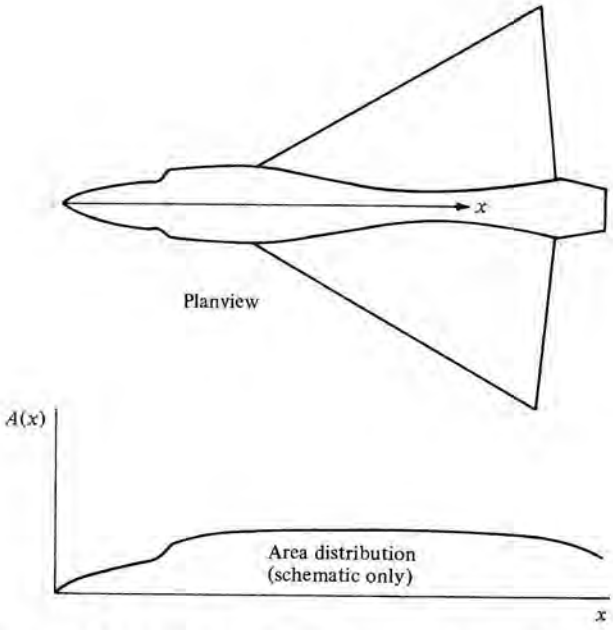

Figure 11.17 A schematic of an area-ruled aircraft.

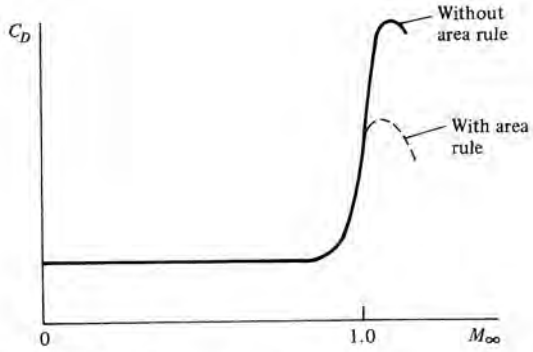

Figure 11.18 The drag-rise properties of area-ruled and non-area-ruled aircraft (schematic only).

11.9 THE SUPERCRITICAL AIRFOIL

Let us return to a consideration of two-dimensional airfoils. A natural conclusion from the material in Section 11.6, and especially from Figure 11.11, is that an airfoil with a high critical Mach number is very desirable, indeed necessary, for high-speed subsonic aircraft. If we can increase M_{cr}, then we can increase $M_{\text{drag-divergence}}$, which follows closely after M_{cr}. This was the philosophy employed in aircraft design from 1945 to approximately 1965. Almost by accident, the NACA 64-series airfoils (see Section 4.2), although originally designed to encourage laminar flow, turned out to have relative high values of M_{cr} in comparison with other NACA shapes. Hence, the NACA 64 series has seen wide application on high-speed airplanes. Also, we know that thinner airfoils have higher values of M_{cr} (see Figure 11.7); hence, aircraft designers have used relatively thin airfoils on high-speed airplanes.

However, there is a limit to how thin a practical airfoil can be. For example, considerations other than aerodynamic influence the airfoil thickness; the airfoil requires a certain thickness for structural strength, and there must be room for the storage of fuel. This prompts the following question: For an airfoil of given thickness, how can we delay the large drag rise to higher Mach numbers? To increase M_{cr} is one obvious tack, as described above, but there is another approach. Rather than increasing M_{cr}, let us strive to increase the Mach number *increment* between M_{cr} and $M_{\text{drag-divergence}}$. That is, referring to Figure 11.11, let us increase the distance between points e and c. This philosophy has been pursued since 1965, leading to the design of a new family of airfoils called *supercritical airfoils*, which are the subject of this section.

The purpose of a supercritical airfoil is to increase the value of $M_{\text{drag-divergence}}$, although M_{cr} may change very little. The shape of a supercritical airfoil is compared with an NACA 64-series airfoil in Figure 11.19. Here, an NACA 64_2-A215 airfoil is sketched in Figure 11.19*a*, and a 13-percent thick supercritical airfoil is shown in Figure 11.19*c*. (Note the similarity between the supercritical profile and the modern

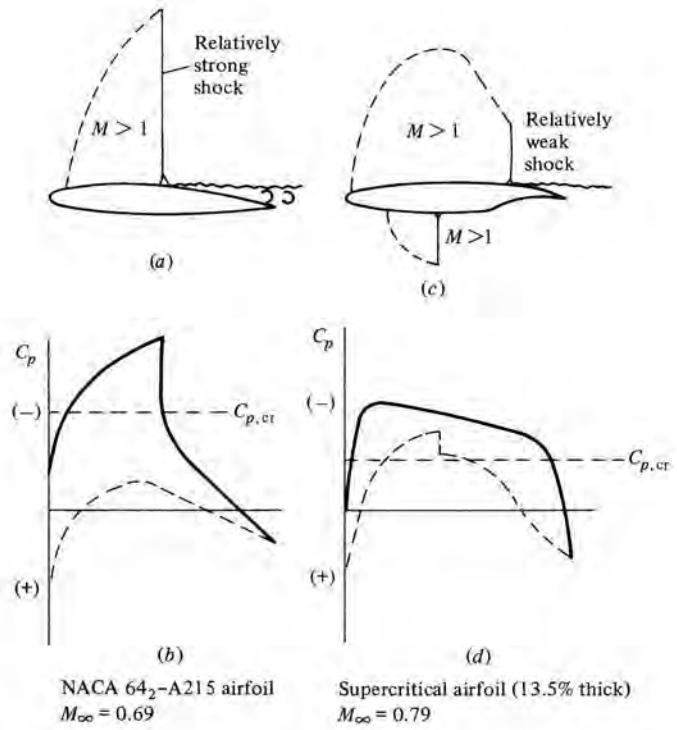

Figure 11.19 Standard NACA 64-series airfoil compared with a supercritical airfoil at cruise lift conditions. *(From Reference 32.)*

low-speed airfoils discussed in Section 4.11.) The supercritical airfoil has a relatively flap top, thus encouraging a region of supersonic flow with lower local values of M than the NACA 64 series. In turn, the terminating shock is weaker, thus creating less drag. Similar trends can be seen by comparing the C_p distributions for the NACA 64 series (Figure 11.19*b*) and the supercritical airfoil (Figure 11.19*d*). Indeed, Figure 11.19*a* and *b* for the NACA 64-series airfoil pertain to a lower freestream Mach number, $M_\infty = 0.69$, than Figure 11.19*c* and *d*, which pertain to the supercritial airfoil at a higher freestream Mach number, $M_\infty = 0.79$. In spite of the fact that the 64-series airfoil is at a lower M_∞, the extent of the supersonic flow reaches farther above the airfoil, the local supersonic Mach numbers are higher, and the terminating shock wave is stronger. Clearly, the supercritical airfoil shows more desirable flow-field characteristics; namely, the extent of the supersonic flow is closer to the surface, the local supersonic Mach numbers are lower, and the terminating shock wave is weaker. As a result, the value of $M_{\text{drag-divergence}}$ will be higher for the supercritical airfoil. This is verified by the experimental data given in Figure 11.20, taken from Reference 32. Here, the value of $M_{\text{drag-divergence}}$ is 0.79 for the supercritical airfoil in comparison with 0.67 for the NACA 64 series.

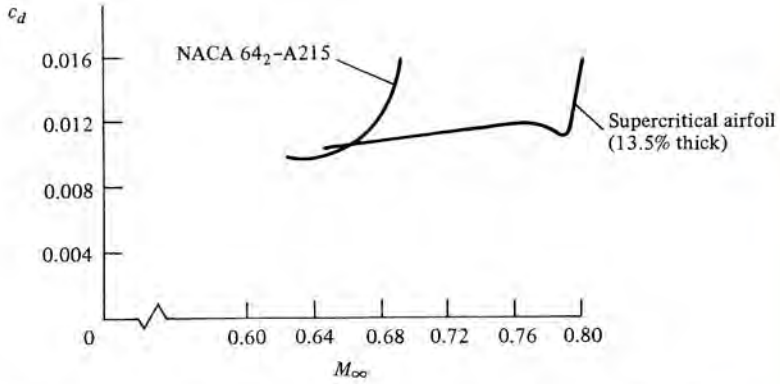

Figure 11.20 The drag-divergence properties of a standard NACA 64-series airfoil and a supercritical airfoil.

Because the top of the supercritical airfoil is relatively flat, the forward 60 percent of the airfoil has negative camber, which lowers the lift. To compensate, the lift is increased by having extreme positive camber on the rearward 30 percent of the airfoil. This is the reason for the cusplike shape of the bottom surface near the trailing edge.

The supercritical airfoil was developed by Richard Whitcomb in 1965 at the NASA Langley Research Center. A detailed description of the rationale as well as some early experimental data for supercritial airfoils are given by Whitcomb in Reference 32, which should be consulted for more details. The supercritical airfoil, and many variations of such, are now used by the aircraft industry on modern high-speed airplane designs. Examples are the Boeing 757 and 767, and the latest model Lear jets. The supercritical airfoil is one of two major breakthroughs made in transonic airplane aerodynamics since 1945, the other being the area rule discussed in Section 11.8. It is a testimonial to the man that Richard Whitcomb was mainly responsible for both.

11.10 CFD Applications: Transonic Airfoils and Wings

The analysis of subsonic compressible flow over airfoils discussed in this chapter, resulting in classic compressibility corrections such as the Prandtl-Glauert rule (Section 11.4), fits into the category of "closed-form" theory as discussed in Section 2.17.1. Although this theory is elegant and useful, it is restricted to:

1. Thin airfoils at small angles of attack
2. Subsonic numbers that do not approach too close to one, that is, Mach numbers typically below 0.7
3. Inviscid, irrotational flow